# The anomalous structures of atmospheric and oceanic variables associated with the frequency of North Pacific winter blocking

Jae-Eun You[1] and Joong-Bae Ahn[1]

Received 2 January 2012; revised 29 March 2012; accepted 21 April 2012; published 6 June 2012.

[1] From Empirical Orthogonal Function (EOF) analysis of the atmospheric and oceanic variables over the North Pacific during the northern hemispheric winter (1960–2009), we were able to determine that the second mode of the EOF is related to North Pacific winter blocking. Our composite analysis reveals that the structures of the variables during winters with contrasting frequencies of blocking events are systematically different and show quite opposite pattern in the North Pacific. During winters with frequent blocking occurrence, a north–south dipole pattern of geopotential height anomaly is formed, and the associated westerly winds are weakened (strengthen) north (south) of 35°N. These factors bring variations of ocean advection and ocean surface heat flux, resulting in a dipole pattern of Sea Surface Temperature (SST), with a warm anomaly north of 35°N and a cold anomaly to the south. The effect of SST on blocking is examined using an Atmospheric General Circulation Model (AGCM) experiment. In the experiment, the SST anomaly related to blocking is applied as a boundary forcing of the AGCM to investigate the effect of SST on the formation of blocking. From the experiment, we also concluded that the winter blocking is not induced by North Pacific SST forcing, although consistent linkage between oceanic and atmospheric variables is evident.

**Citation:** You, J.-E., and J.-B. Ahn (2012), The anomalous structures of atmospheric and oceanic variables associated with the frequency of North Pacific winter blocking, *J. Geophys. Res.*, *117*, D11108, doi:10.1029/2012JD017431.

## 1. Introduction

[2] Blocking is defined as a stagnant or slowly moving quasi-stationary ridge that normally builds up over the North Pacific and North Atlantic during northern hemispheric winter. This synoptic phenomenon is usually related to several extreme weather events such as an extraordinarily warm or cold and wet or dry winter [*Matsueda et al.*, 2009; *Buehler et al.*, 2011]. For these reasons, a better understanding and prediction of the blocking phenomenon is necessary.

[3] Several indices have been used as objective methods in order to detect blocking. The most popular method is an index that uses meridional geopotential height gradients. The index was originally defined by *Rex* [1950] and has been used in many studies [e.g., *Lejenäs and Øakland*, 1983; *Tibaldi and Molteni*, 1990; *Trigo et al.*, 2004; *Barriopedro et al.*, 2006]. In addition, various indices have been defined, such as the blocking intensity index, described as the average intensity of the daily maximum heights in an event [*Lupo*, 1997]; the index using meridional potential temperature gradients [*Pelly and Hoskins*, 2003]; and the Blocking Index (BI) with two dimensions [*Diao et al.*, 2006]. The results of statistical characteristics analysis of northern hemisphere blocking via the blocking indices have shown that blocking is strong and long-lasting in the North Atlantic and North Pacific, especially in the winter [*Wiedenmann et al.*, 2002; *Barriopedro et al.*, 2006].

[4] In terms of blocking, many studies have emphasized the role of internal atmospheric transient eddies [e.g., *Kalnay-Rivas and Merkine*, 1981; *Shutts* 1983; *Holopainen and Fortelius*, 1987; *Nakamura et al.*, 1997; *Huang et al.*, 2002]. Whereas, some studies have proposed that ocean heat forcing is able to reinforce blocking [e.g., *Kung et al.*, 1990; *Huang et al.*, 2002; *Tilly et al.*, 2008].

[5] According to general air-sea interaction studies, it is well known that atmospheric forcing has an influence on Sea Surface Temperature (SST) at middle and high latitudes [e.g., *Frankignoul*, 1985; *Liu et al.*, 2006; *Alexander*, 2010]. On the other hand, many experiments have been conducted to assess atmospheric changes in response to SST anomalies at midlatitudes [e.g., *Lau and Nath*, 1990; *Peng and Whitaker*, 1999; *Rodwell et al.*, 1999; *Huang et al.*, 2002; *Liu and Wu*, 2004; *Ferreira and Frankignoul*, 2005]. Regarding experiments carried out to examine the influence of SST on blocking formation, *Kung et al.* [1990] conducted a simulation of blocking formation for January 1979, applying global observed SST anomalies as a boundary condition of the General Circulation Model (GCM). *Tilly et al.* [2008]

[1]Division of Earth Environmental System, Pusan National University, Busan, South Korea.

Corresponding author: J.-B. Ahn, Division of Earth Environmental System, Pusan National University, Jangjeon 2-dong, Geumjeong-gu, Busan 609-735, South Korea. (jbahn@pusan.ac.kr)


0148-0227/12/2012JD017431

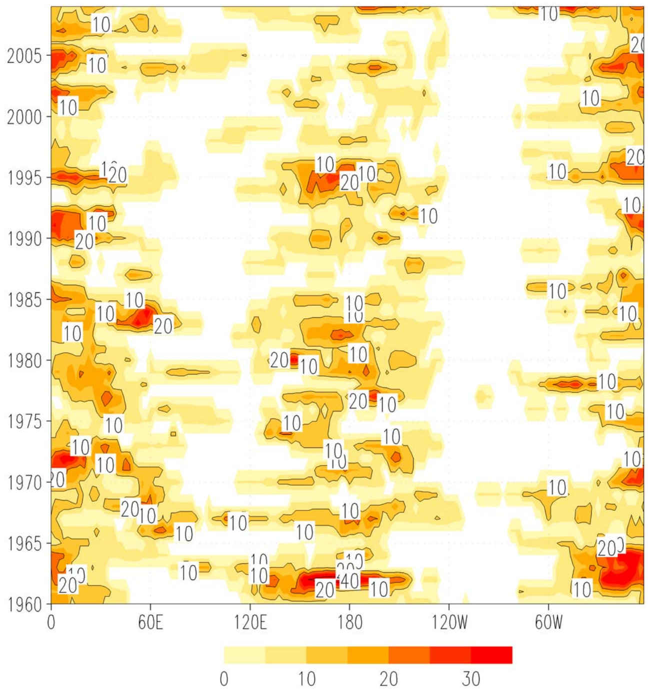


**Figure 1.** Distribution of the winter blocking frequency in the longitude and time domain.

proposed that diabatic processes contribute to the two cases of Southern Hemisphere blocking intensification through the theoretical study using vorticity equations; however, the previous studies on heating as a contributor of blocking were not generalized. Furthermore, experiments to determine how blocking formation is affected by midlatitude SST have not yet been carried out. According to previous studies, the atmospheric response affected by SST anomalies is small in midlatitudes [*Liu and Wu*, 2004], and has different characteristics depending on experimental conditions such as forcing areas, experimental period, and model types. Regarding the feedback between atmosphere and ocean, however, some studies [*Palmer and Zhaobo*, 1985; *Watanabe*, 2001; *Liu and Wu*, 2004] insisted that there is positive feedback between warm SST and higher pressure through the role of surface heat flux.

[6] In this study, we considered the possibility that blocking has an effect on the ocean, the potential of blocking formation influenced by SST anomaly associated with the blocking, and the probability that blocking occurs through the interaction between the atmosphere and the ocean. To accomplish this, first of all, we found the blocking mode though EOF analysis of the atmosphere and ocean fields during northern hemispheric winter; based on this, we analyzed composite reanalysis fields. Through this analysis, we assessed all the possibilities mentioned above.

[7] In section 2, we introduce the data and method used to calculate the blocking index, while in section 3, we determine the blocking mode using Empirical Orthogonal Function (EOF) analysis. In section 4, we investigate the anomalous structures of variables associated with the blocking frequency through the analysis of the anomaly composites. In section 5, we study the possibility of an effect of SST using an Atmospheric GCM (AGCM). A summary and conclusion are given in section 5.

## 2. Data and Method

### 2.1. Data

[8] The data used in the study are reanalysis data provided by the NOAA Earth System Research Laboratory and ECMWF's Ocean ReAnalysis (ORA). The National Centers for Environmental Prediction/National Center for Atmospheric Research (NCEP/NCAR) reanalysis-1 data with a 2.5° × 2.5° resolution are used for geopotential height and wind for the period from 1960 to 2009. In addition, NOAA-CIRES 20C reanalysis-2 data constructed on a 1.9° × 1.9° grid for the period from 1960 to 2007 are used for the estimation of the radiation and heat fluxes at the ocean surface.

[9] As for the ocean variables, ORA products are used for SST and currents for the period between 1960 and 2008. The data has 29 vertical levels from 5 to 5250 m, and is organized by horizontal 1° × 1° grids. NOAA Optimum Interpolation SST data from 1982 to 2008 with 1° × 1° grids are also used.

### 2.2. Definition of Blocking Index

[10] In this study, we defined blocking from an index that considers meridional geopotential height gradients derived from the criterion of *Barriopedro et al.* [2006] which is based on the method proposed by *Tibaldi and Molteni* [1990]. This index was calculated using the daily mean 500 hPa geopotential height for 50 winters (1960–2009) as follows:

$$GHGN(\lambda) = \frac{Z(\lambda, \phi_N) - Z(\lambda, \phi_0)}{\phi_N - \phi_0}, \quad GHGS(\lambda) = \frac{Z(\lambda, \phi_0) - Z(\lambda, \phi_S)}{\phi_0 - \phi_S}, \tag{1}$$

where $Z(\lambda, \phi)$ is the 500 hPa geopotential height at $(\lambda, \phi)$, and GHGN($\lambda$) and GHGS($\lambda$) are southern and northern 500 hPa geopotential height gradients, respectively, at a given latitude ($\phi$) as follows:

$$\begin{aligned} \phi_N &= 77.5°N + \Delta, \\ \phi_0 &= 60.0°N + \Delta, \\ \phi_S &= 40.0°N + \Delta, \\ \Delta &= -5.0°, -2.5°, 0.0°, 2.5°, 5.0°. \end{aligned} \tag{2}$$

[11] The five values for $\Delta$ were applied, and five results for GPGN($\lambda$) and GPGS($\lambda$) were computed, respectively. A longitude is considered to be blocked when GHGN($\lambda$) is less than $-10$ gpm per latitude with a GHGS($\lambda$) larger than 0 for at least one case among the five different latitudes:

$$GHGN(\lambda) < -10gpm \cdot lat^{-1}, \quad GHGS(\lambda) > 0. \tag{3}$$

[12] Furthermore, such condition must continue over five or more days to be considered as blocking. The blocking frequency (BF) is defined as the ratio of the blocking days to 90-days of a winter [*Barriopedro et al.*, 2006] between 1960 and 2009.

[13] In Figure 1, the BF displayed in the longitude and time (year) domain has a high value in the North Pacific and

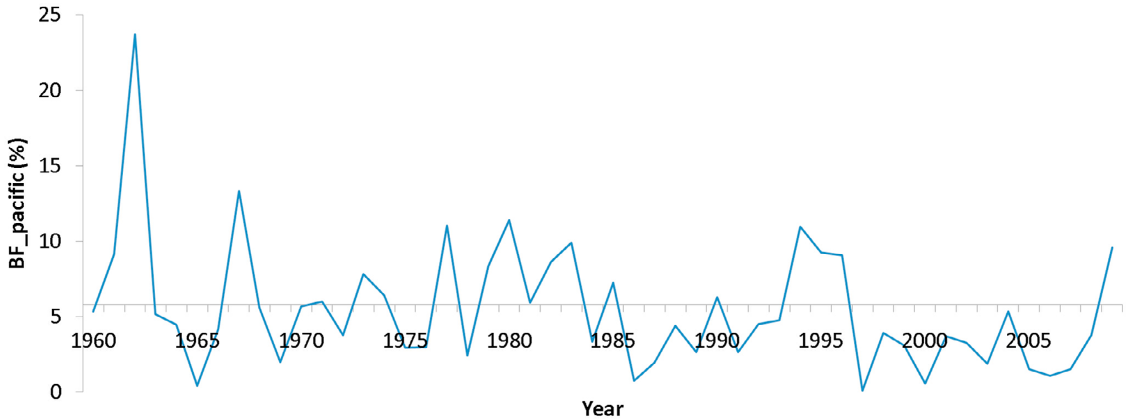


**Figure 2.** Interannual variability of averaged BF over the region of 110°E–120°W, 1960–2009. The horizontal line indicates the average for 50 years.

North Atlantic, with the respective maxima located along 180° and 0°. In the case of the North Pacific, blocking was significantly decreased from the late 1980s to the early 1990s and from 1997 to 2008, whereas there were no notable changes in the North Atlantic. The North Pacific blocking index, BF_pacific, was defined as the average over the region of 110°E–120°W to analyze the North Pacific blocking in this study. Figure 2 shows the time series of BF_pacific. It has a range from 0 to 24% (0–22 days), and the average of 50 winters is 5.5% (5 days). The 20 winters with a higher BF_pacific than average are defined as winters of high blocking frequency (HBW), and the 30 winters with a lower BF_pacific than average are defined as winters of low blocking frequency (LBW); these are compared in section 4.

## 3. Blocking Mode and EOF Analysis of the North Pacific in Winter

[14] To determine the dominant modes of North Pacific climate variability, EOF analysis has been performed for geopotential height (GPH), the U component of wind (U-wind), temperature at 500 hPa, and SST. The analysis domain is 110°E–120°W, 20–75°N and the trend was removed prior to analysis.

[15] Table 1 shows the correlation coefficient between BF_pacific and EOF time series of the first two modes for each variable. Except for U-wind, the variables were not correlated with BF_pacific in the first EOF mode. It is generally known that the first mode has a significant relation with Arctic Oscillation (AO) [e.g., *Thompson and Wallace* 1998]. Whereas, in the second EOF mode, the correlation coefficient between BF_pacific and the SST is −0.4, the geopotential height is 0.66, the U-wind is −0.55, and the temperature is −0.62. Therefore, it can be inferred that the second EOF mode is quite related to blocking.

[16] As a result of spatial pattern analysis for the same variables, the composite anomaly field of HBW and LBW displayed a similar pattern to the second EOF mode, describing 17–22% of the total variance for each variable (Figure 3). If we compare the two kinds of patterns, the positive and negative signs of SST and U-wind change along 35°N and 55°N, while geopotential height and temperature change in terms of the sign along 45°N. The result seems to differ slightly (not shown) if we use different reanalysis data (e.g., Extended Reconstructed SST (ERSST)), but variations in scale as well as the positive and negative areas of the two patterns resemble each other.

[17] According to the results, the second EOF mode is defined as the blocking mode in North Pacific. We assess how meteorological variables are connected in the blocking mode using the analysis of composite anomaly fields for HBW and LBW in the following section.

## 4. The Anomalous Structures of Variables Associated With North Pacific Winter Blocking

### 4.1. Height and Wind Change Associated With Blocking

[18] Figures 4a and 4b show the vertical cross-sections of composite geopotential height anomaly for HBW along 60°N and 180°, respectively. The blocking has a barotropic structure in the vertical, with a positive height anomaly from ground to upper levels. Meanwhile, there is a dipole-like pattern whereby there is a negative height anomaly south of 45°N along the 180°, and a positive height anomaly above that latitude.

**Table 1.** Correlation Coefficients Between the BF_Pacific and the EOF PC Time Series of Each Variable at 500 hPa for the Winter Season

| | SST | | GPH | | U-wind | | Temperature | |
|---|---|---|---|---|---|---|---|---|
| Correlation | pc1 | pc2 | pc1 | pc2 | pc1 | pc2 | pc1 | pc2 |
| BF_pacific | 0.11 | −0.40 | 0.22 | 0.66 | −0.46 | −0.55 | −0.10 | −0.62 |

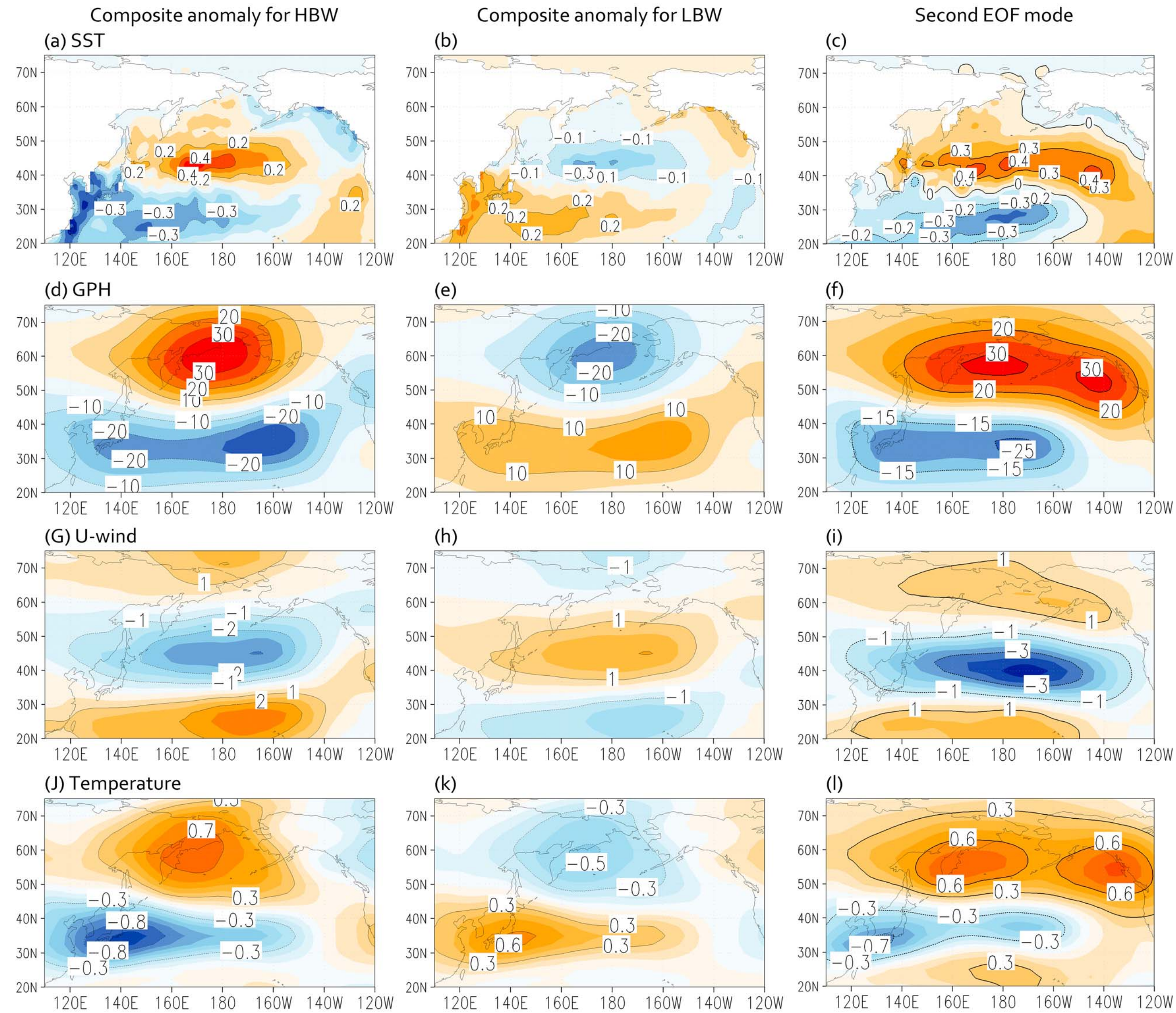


**Figure 3.** Composite anomaly for winters with (a, d, g, j) higher BF, with (b, e, h, k) lower BF than the 50-year average, and the second EOF mode of (c) SST, (f) GPH, (i) U-wind, and (l) temperature at 500 hPa.

[19] Figure 5 shows the climatological mean and the composite anomaly fields for HBW and LBW of the geopotential height at surface, at 500 hPa, and at 300 hPa. The composite anomalies in the HBW and LBW have opposite patterns, as shown in the figure. Thus, we can infer that the local circulations in the two cases are quite opposite and that the blocking is systematic feature.

[20] During the HBW, the flows meander more at the upper level; at the same time, the surface Aleutian Low is weakened and moves southward. Therefore, the meridional height gradients are reduced centering at 45°N, and are increased around 25°N, with positive anomaly located at high latitude and negative anomaly located at low latitude. In the LBW, however, the zonal flow becomes strong at the upper level and the surface Aleutian Low is strengthened and moves northward. Therefore, the meridional height gradients are increased around 45°N and reduced around 25°N.

[21] The zonal wind also has opposite patterns in the HBW and LBW (Figure 6) in association with the geopotential height. The composite anomaly fields for the HBW of geopotential height (Figure 5) showed that the center of positive anomaly was along 60°N, and maximum negative anomaly was along 35°N, so the meridional geopotential height difference is reduced, particularly at 35°N–60°N. This result in reduced westerly winds over that area, while the westerly winds are strengthened in relatively low latitudes around 25°N. Therefore, the westerly wind bands in midlatitude tend to move southward, corresponding to the area of large geopotential height gradients. In contrast, in LBW, the meridional geopotential height difference is developed compared to climatology over 35–60°N. Associated with this, the westerly wind band strengthens and appears more northward than climatology.

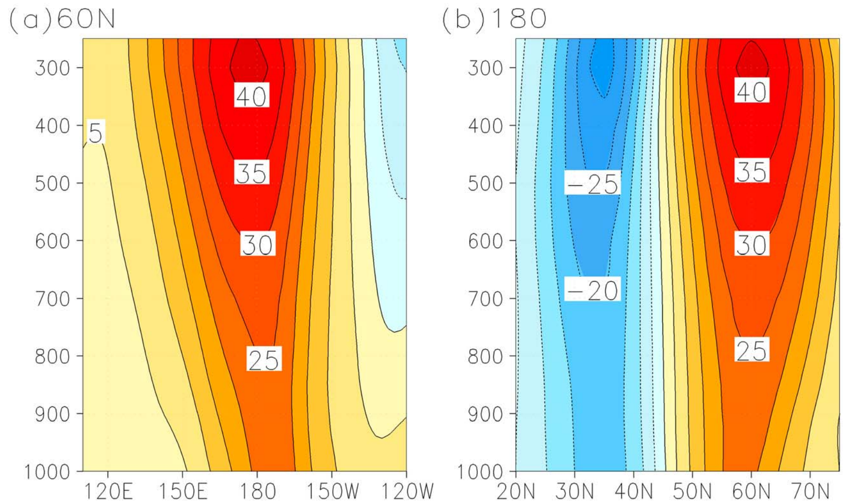


**Figure 4.** The composite geopotential height anomaly for HBW on a vertical cross-section along (a) 60°N and (b) 180°.

## 4.2. The SST Change Associated With Blocking

[22] Figure 7 shows the climatological mean and the composite anomaly fields in the HBW and LBW of SST. During the period, in HBW and LBW, the composite SST anomaly fields display opposite patterns to each other. The center of positive anomaly is located along 43°N, and that of negative anomaly is located along 25°N in HBW, similar to the zonal wind anomaly field. Figures 8a and 8b illustrate vertical cross-sections of the composite sea temperature anomaly and current vector anomaly in HBW along the east–west direction and along the north–south direction, respectively. Sea temperature anomaly related to blocking appears systematically, to a depth of approximately 400 m. A similar anomaly pattern is formed almost uniformly from

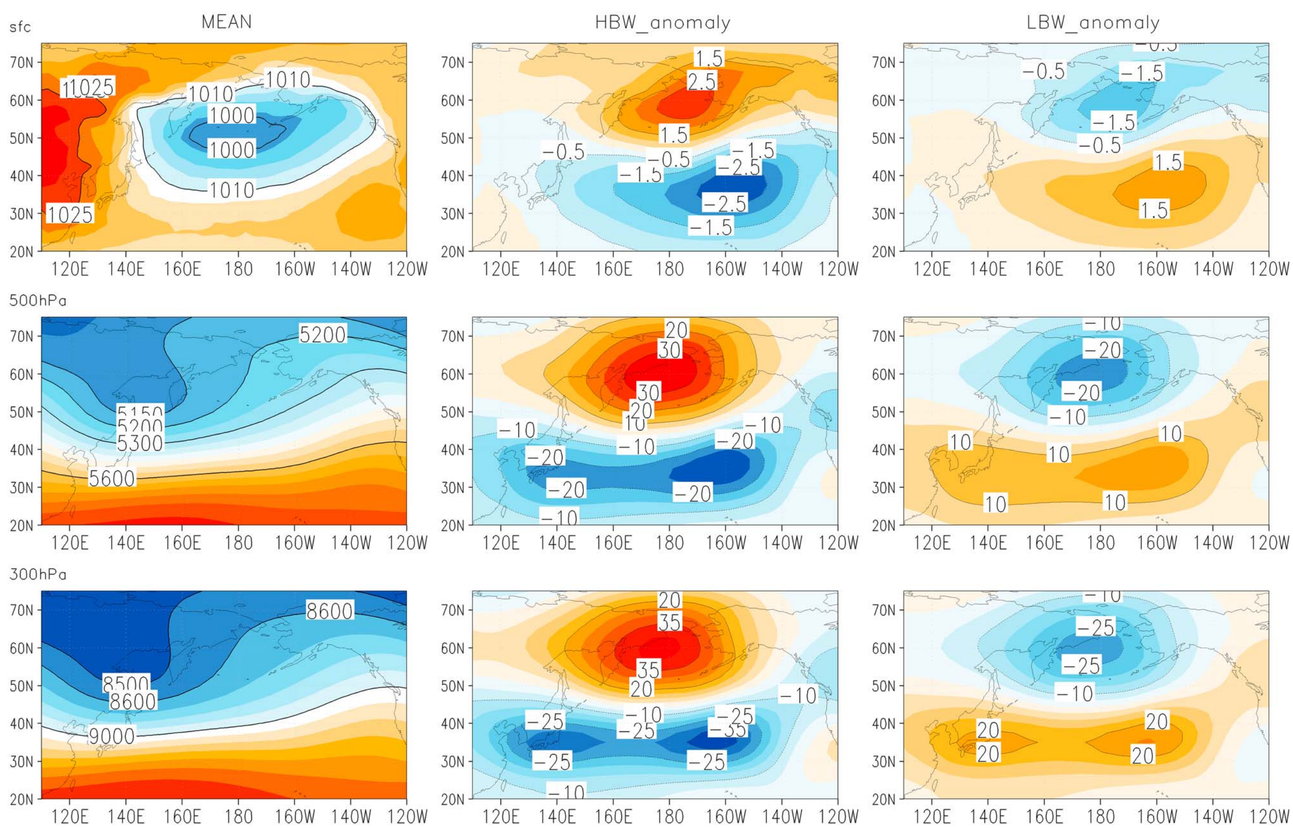


**Figure 5.** The (left) climatological mean fields of geopotential height, the (center) composite anomaly for HBW and (right) LBW at the (top) surface, (middle) 500 hPa, and (bottom) 300 hPa.

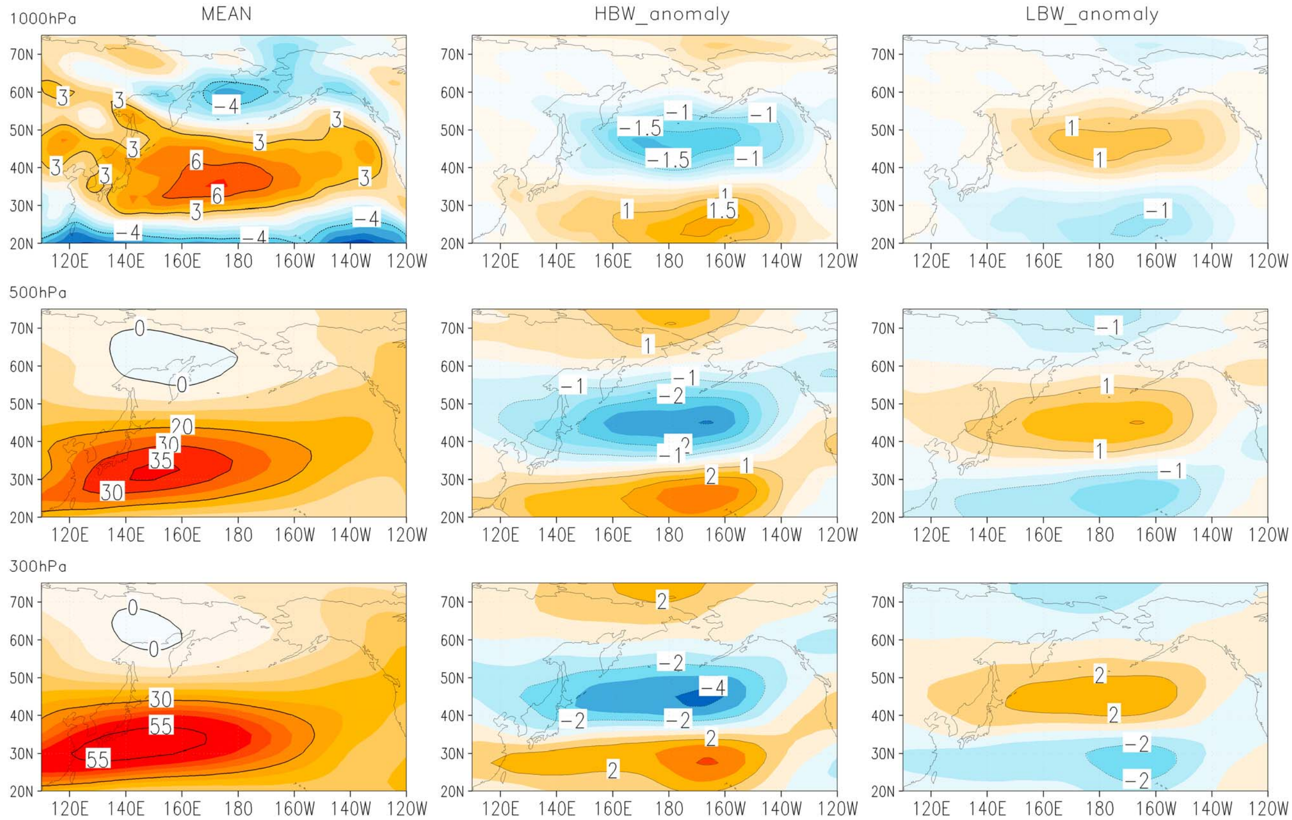


**Figure 6.** As in Figure 5, but for U-wind.

the surface to a depth of approximately 100 m. The surface wind causes the current vector anomaly near the surface, particularly for meridional current. Furthermore, at a depth of 50 m below, anomalous downward (upward) vertical motion appears in the velocity convergence (divergence) area.

[23] In this study, to determine which physical processes contribute to the formation of the SST anomaly, first, we estimated surface heat flux as follows:

$$H = H_{SR} - (H_{LR} + H_{SH} + H_{LH}). \tag{4}$$

[24] The net downward surface heat flux (H) is the sum of net downward solar radiation flux ($H_{SR}$), net upward long wave radiation flux ($H_{LR}$), net upward sensible heat flux ($H_{SH}$), and net upward latent heat flux ($H_{LH}$); the climatological net heat flux associated with the two anomalies during HBW and LBW is shown in Figure 9. In HBW, more upward heat is seen in low latitudes west of 150°W, but there are downward anomalies in the other areas of the North Pacific, resulting in the increase of sea temperature around the area of 160°E–160°W, 40°N–60°N. The net downward surface heat flux anomaly is primarily formed by $H_{SH}$ and $H_{LH}$ under the influence of wind. At high latitude a lesser amount of heat is exported where the surface westerly wind is weakened from the ocean surface and contributes to the increase of sea temperature. In contrast, for low latitudes, more heat is exported where wind is strengthened and contributes to cooling. However, the composite anomaly of net downward surface heat flux has different patterns compared with that of SST, including the location of the SST anomaly core along the 43°N.

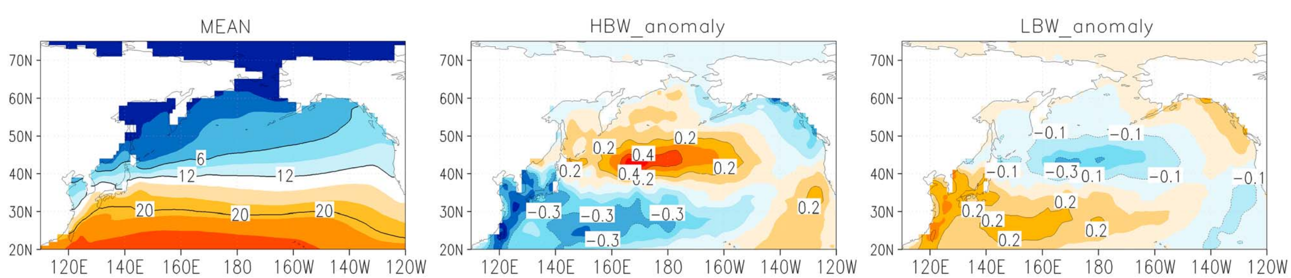


**Figure 7.** The (left) climatological mean fields of SST; the (middle) composite anomaly for HBW and (right) LBW at the surface.

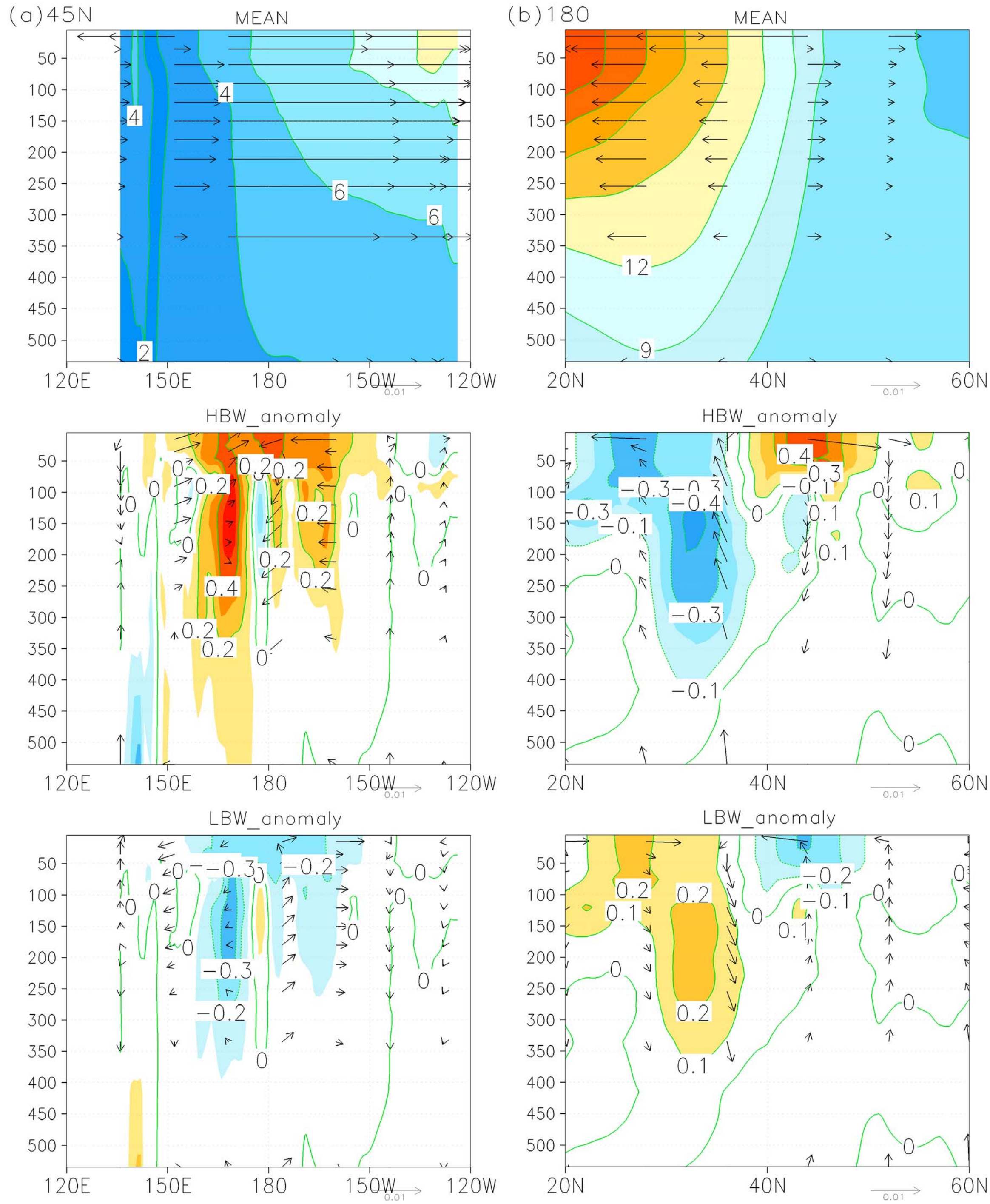


**Figure 8.** A vertical cross-section of sea temperature and (a) zonal (unit: m/s) and vertical current (unit: $10^4$ m/s) as vectors along 45°N and (b) meridional (unit: m/s) and vertical current (unit: $10^4$ m/s) as vectors along 180°. The climatological mean fields (top); composite anomaly for HBW (middle) and LBW (bottom).

[25] In order to address the discrepancy, the ocean heat advection is considered as another factor that can affect SST and is estimated as follows:

$$\text{Zonal heat advection} = -\rho C_p \int_{z_b}^{0} \bar{U}\frac{\partial \bar{T}}{\partial x}dz, \tag{5}$$

$$\text{Meridional heat advection} = -\rho C_p \int_{z_b}^{0} \bar{V}\frac{\partial \bar{T}}{\partial y}dz, \tag{6}$$

$$\text{Vertical heat advection} = -\rho C_p \int_{z_b}^{0} \bar{W}\frac{\partial \bar{T}}{\partial z}dz. \tag{7}$$

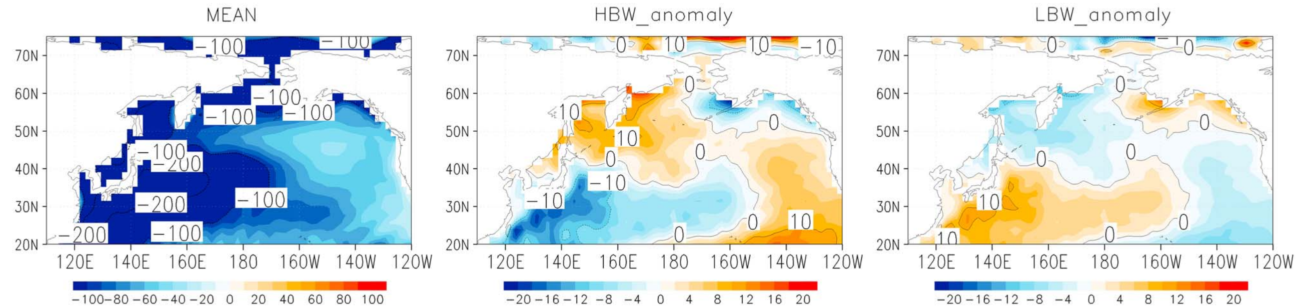


**Figure 9.** As in Figure 7, but for downward net surface heat flux (unit: $10^{-7}$ Wm$^{-2}$ 3 month).

[26] Here, $\rho$ is the density, 1022.4 $Kg \cdot m^{-3}$; $C_p$ is the specific heat of the ocean, 3940 $J \cdot Kg^{-1}{}^{\circ}C^{-1}$, and $z_b$ is 30 m as the sub-surface. All flux terms have positive value when they contribute to the heat gain in a unit column of upper ocean ($0 - z_b$). As an example, zonal heat advection was produced by integrating the product of the mean zonal current ($\bar{U}$) and the zonal temperature gradient ($\partial\bar{T}/\partial x$) into the unit volume vertically integrated from the surface to a depth of 30 m. Each heat advection is shown in Figure 10. The most variable flux due to blocking is meridional heat advection. During the HBW, meridional heat advection reinforces cooling to the south of 35°N, and the heating to the north of 35°N. In particular, it contributes to heating in the areas of 37°N–47°N and 160°E–170°W. The variation of anomalous westerly wind, as shown in section 4.1, contributes to the formation of anomalous meridional heat advection. The North Pacific current flows mainly from the north to the south Pacific in the meridional mean fields, but during the HBW, the weakened westerly wind results in less transport of cold water from high latitude; therefore, sea temperature increases to the north of 35°N. In the lower latitude, conversely, the strengthened westerly wind leads to stronger cold advection, and this contributes to the cooling of the sea temperature.

[27] The sum of net downward heat flux and heat advections for HBW and LBW are shown in Figure 11. Comparing with the SST anomalies represented in Figure 7, we can

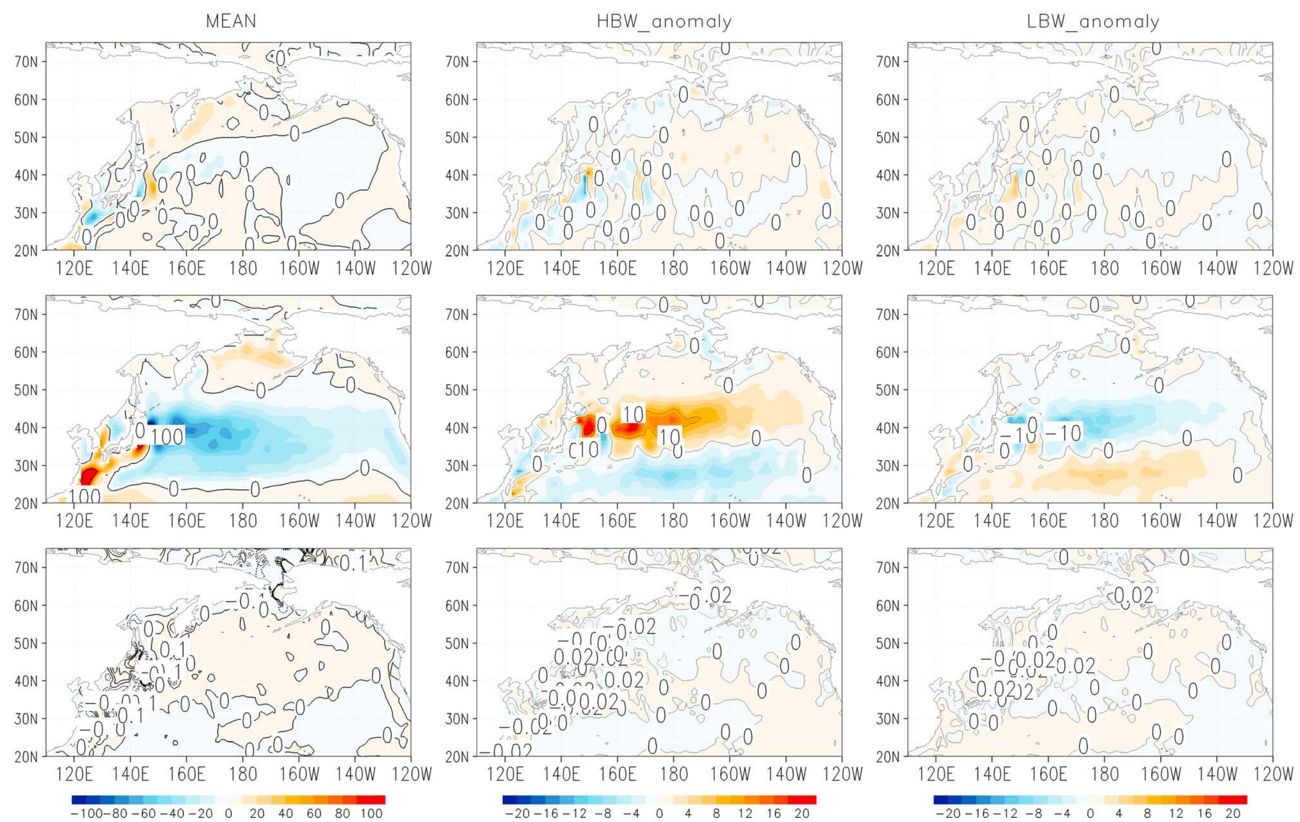


**Figure 10.** As in Figure 7, but for zonal heat advection (upper), meridional heat advection (middle), and vertical heat advection (bottom) (unit: $10^{-7}$ Wm$^{-2}$ 3 month).

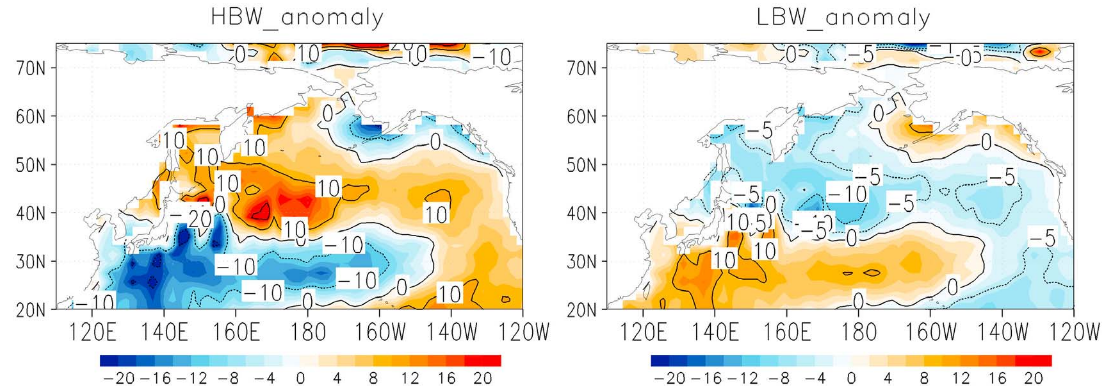


**Figure 11.** Composite anomaly for (left) HBW and (right) LBW of the sum of net downward heat flux and heat advections.

see that the positive and negative area and the region located at the maximum and minimum value are similar. It implies that the factor that contributes most to the change in sea temperature is meridional heat advection; and that surface heat flux also partially affects the temperature near the surface. Thus, these changes related to blocking seem to eventually produce the dipole pattern of anomalous SST.

### 4.3. The Atmospheric Response Experiment Using AGCM

[28] *Lau and Nath* [1990] imposed a warm SST anomaly forcing in a particular area of North Pacific (rectangle centered at 31.5°N, 161°W) using AGCM. They argued that in the result of the experiment, a positive height anomaly of the barotropic structure may be formed in the north region of the forcing area. In this study, we examine whether the dipole pattern of SST anomaly associated with blocking can influence the formation of blocking using AGCM experiments. NCAR/CCM3 AGCM was used for the experiment. The horizontal resolution of CCM3 is spectral T42 (approximately 2.8125° Gaussian grid), and vertically it has 18 hybrid sigma-pressure levels. The model includes a land surface model (LSM) that employs six vertical levels.

[29] Two kinds of experiments were performed using SST as the boundary condition for AGCM. The control experiment (CE) used the climatology of SST, while the transient blocking experiment (TBE) used dipole SST anomalies related to HBW and LBW blockings added to climatological SST. We investigated whether changes in SST can influence the formation of blocking by comparing the results of the two kinds of experiments.

[30] Long-term integration was performed for 30 years starting from on arbitrary year (January 15, 2009 in our experiment) under given climatological monthly mean SST averaged over 1982 to 2008 as the lower boundary condition, so that the atmosphere reaches quasi-equilibrium state sufficiently. Then, the climatology SST was given continuously as the lower boundary condition for CE from the 31st year to February of 32nd year. The SSTs related to HBW and LBW (Figure 12) were applied for the AGCM as lower boundary conditions for the same period (Figure 13). Since the SST anomaly related to strong blocking can be three times larger than the composite case, the 3-time larger anomaly forcings related to blocking were gradually imposed from June to winter (December–February). The results of the experiments were analyzed for three months from December of the 31st year to the next February. Figure 14 shows the 500 hPa geopotential height anomalies, and Figure 14a shows the result of the experiment (TBE (HBW) – CE) applied to the SST anomaly associated with HBW as forcing, in which a positive anomaly appears centering on the Kamchatka Peninsula. Figure 14b illustrates the result of the experiment given the SST anomaly related to LBW as forcing, and a stronger anomaly appears in a region similar to the result related to HBW. As shown in the figure,

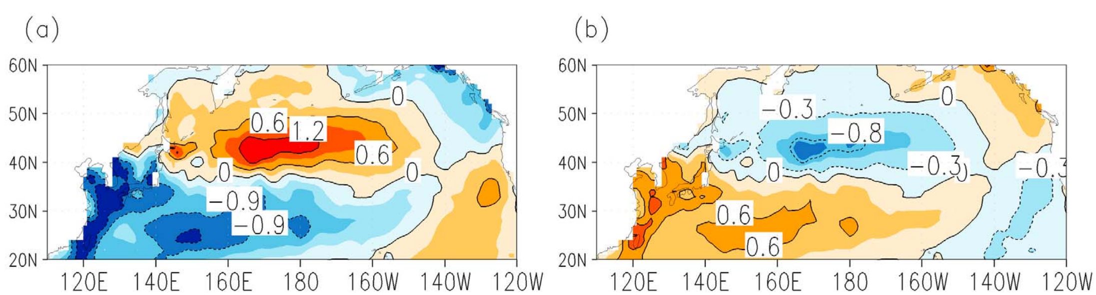


**Figure 12.** SST forcing related to (a) HBW and (b) LBW.

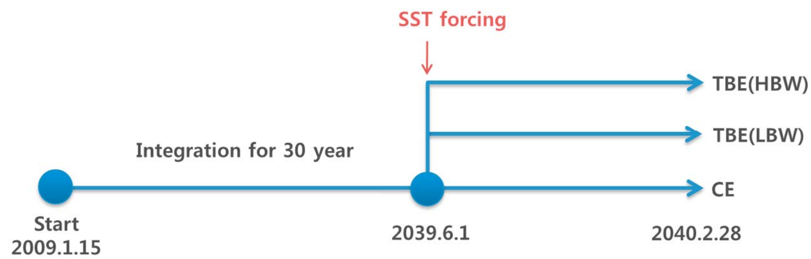


**Figure 13.** Experimental design.

systematic changes related to blocking such as those discussed in Section 4.1 were not reproduced in the experimental result with SST forcing. Therefore, it can be considered that midlatitude SST forcing did not act on the formation of blocking.

[31] Hence, we analyzed the result of CE where SST forcing was not applied to examine whether blocking can be formed by other factors such as atmospheric internal variability regardless of SST forcing. Figure 15 represents the winter mean 500 hPa geopotential height anomalies of CE integration for 29 years. The spatial correlation coefficients between the spatial patterns of CE for each year and the composite anomaly of 500 hPa geopotential height associated with HBW are shown. In the results of CE, a blocking-like pattern that had a spatial correlation coefficient higher than 0.37, 95% level of confidence, appeared five times. Meanwhile, in the NCEP/NCAR reanalysis data, the phenomenon appeared eight times from 1981 to 2009 (Figure 16). From this experiment, we found that blocking patterns appearing in real atmosphere occurred in the model despite the fact that only the climatological SST was applied. It implies that the winter blocking is not induced by the North Pacific SST forcing. Instead, as was reported by several papers, other factors such as internal dynamics of atmosphere [e.g., *Kalnay-Rivas and Merkine*, 1981; *Shutts* 1983; *Holopainen and Fortelius*, 1987; *Nakamura et al.*, 1997], surface boundary forcing due to snow cover and sea-ice [e.g., *Lee and Jhun*, 2006] and anomalous equatorial SST forcing associated with El Nino and La Nina [e.g., *Renwick and Wallace*, 1996; *Wiedenmann et al.*, 2002] can be alternatives to explain the generation mechanism of the North Pacific winter blocking.

## 5. Summary and Conclusion

[32] In this study, the possibility of a winter blocking effect on the ocean over the North Pacific and the probability of the ocean's role in blocking were examined. EOF analyses were carried out for major atmospheric and oceanic variables in winter over the North Pacific. From these analyses, we discovered that the second mode is related to North Pacific blocking in winter. The second mode showed a similar pattern to the composite anomaly fields of HBW and LBW based on the blocking classification of *Barriopedro et al.* [2006]. The composite anomaly fields of HBW and LBW for different atmospheric and oceanic variables have exactly the opposite sign to each other. This means that blocking and its influence appear systematically in the North Pacific.

[33] The geopotential height has a dipole-like structure in HBW (LBW) that shows positive (negative) anomaly at high latitude and negative (positive) anomaly at low latitude. Thus, the meridional height gradients are reduced, and westerly wind weakens in HBW. The mean surface ocean current flows southeastward in the North Pacific, but the weakened westerly wind results in less transport of cold water from high latitude. In addition, the reduced wind speed induces a lesser amount of upward heat flux at the ocean surface. Thus, anomalous warm SST was produced at midlatitude of 35–55°N. In contrast, increased meridional height gradients and strengthened westerly wind eventually cause a

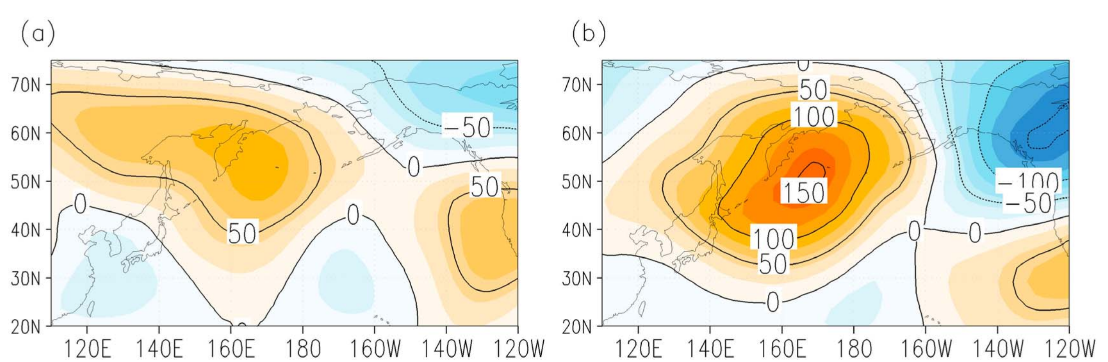


**Figure 14.** The 500 hPa geopotential height anomalies as the experimental result with SST forcing related to (a) HBW and (b) LBW.

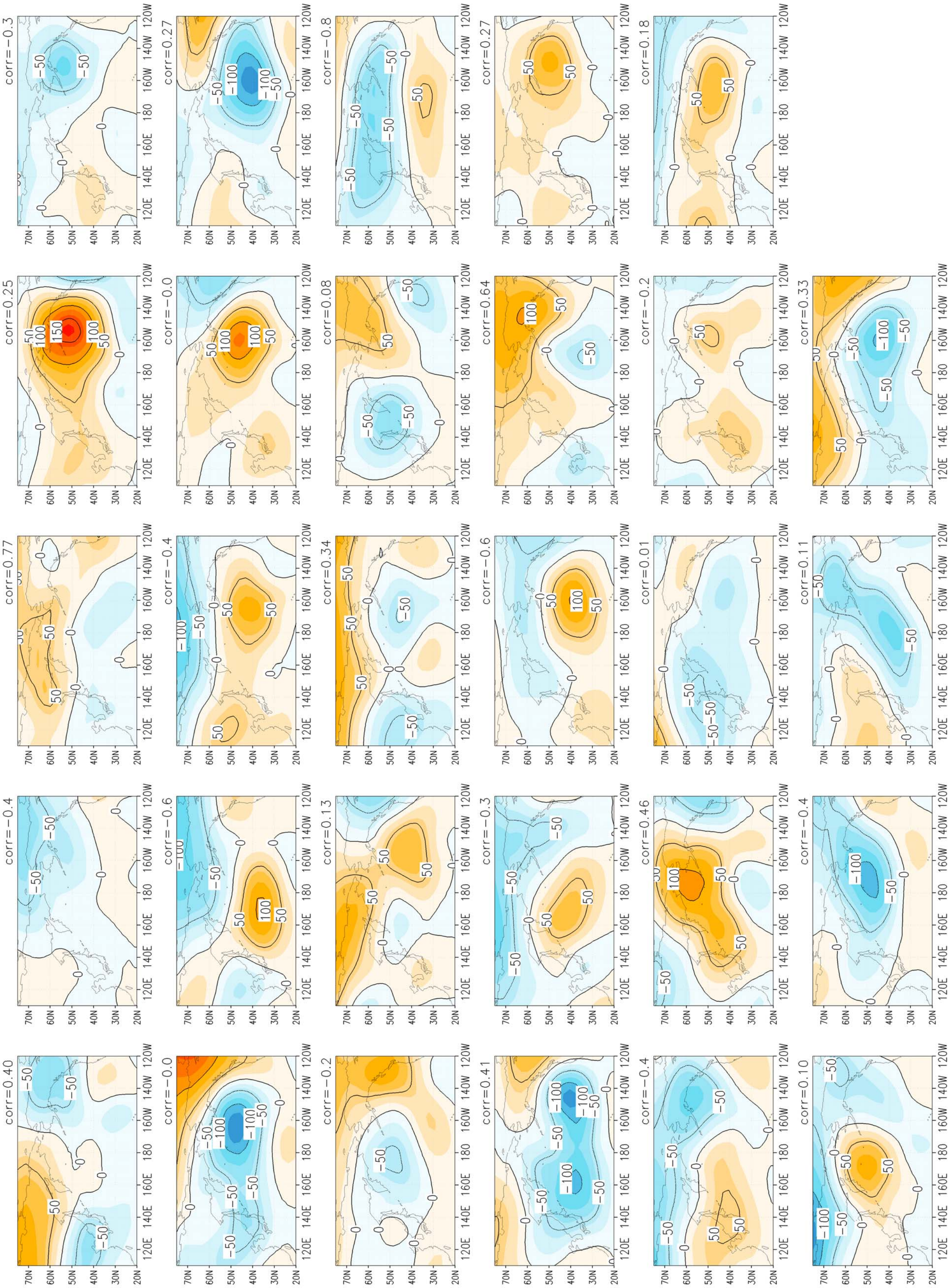


**Figure 15.** The winter mean 500 hPa geopotential height of the CE result and spatial correlation between each CE result for 2009–2037 and composite anomaly field of HBW.

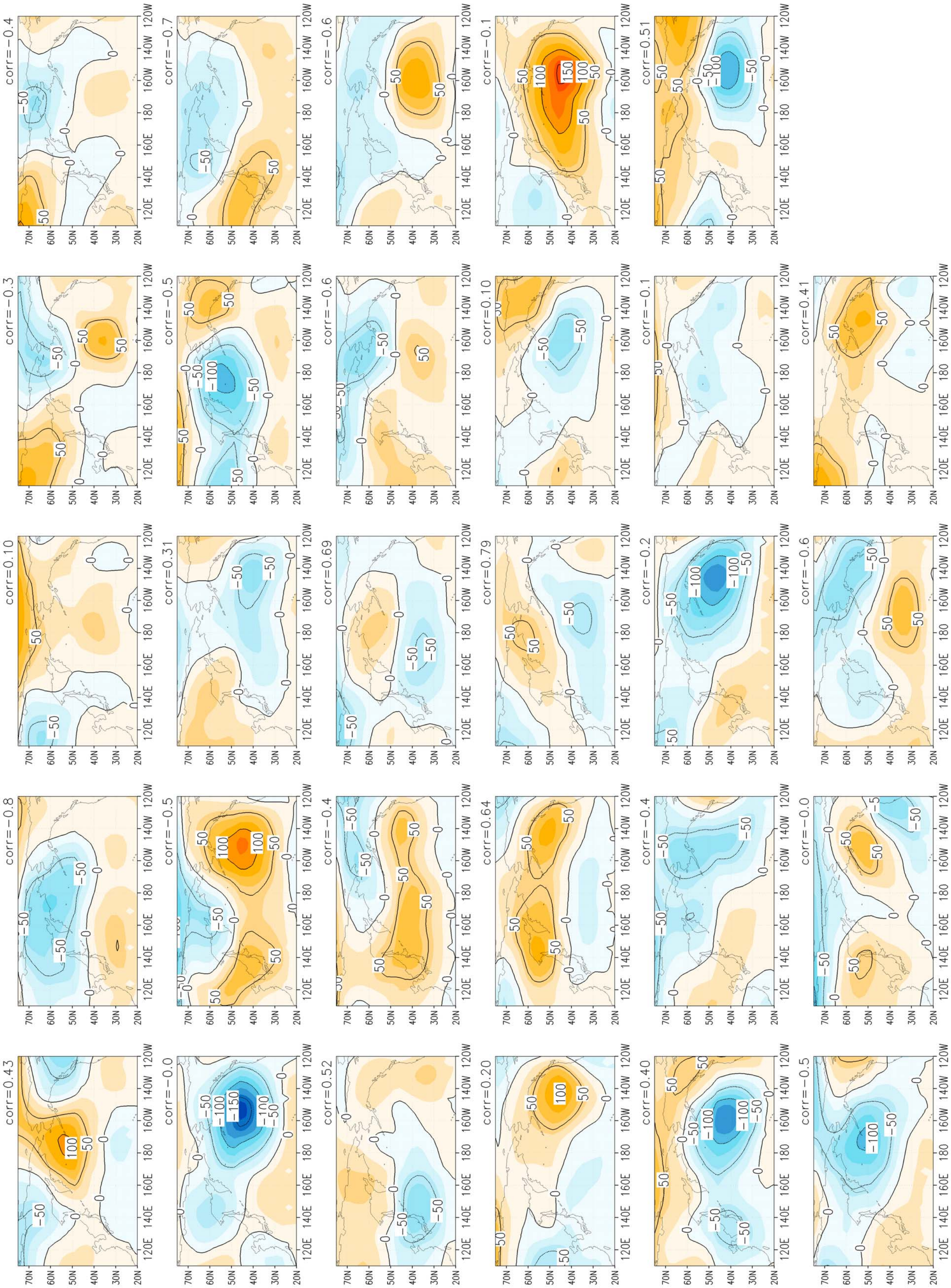

**Figure 16.** The reanalysis data for the winter mean 500 hPa geopotential height and spatial correlation between each pattern for 1981–2009 and composite anomaly field of HBW.

release of more heat flux upward and produce cold advection, resulting in anomalous cold SST at latitudes lower than 35°N, west of 150°W. Thus, SST anomaly related to HBW and LBW has a dipole-like pattern through the atmospheric blocking influence.

[34] Also, in this study, AGCM experiments had been conducted with SST forcing related to blocking to understand whether SST can play a role in the creation and maintenance of blocking. According to our results, systematic atmospheric response to the dipole pattern of SST forcing related to blocking did not appear as shown in the observation. Furthermore, a pattern of atmospheric anomaly similar to blocking also appeared without North Pacific SST forcing in the result of the control experiment for 29 years. Hence, we suggest that the winter blocking is not induced by North Pacific SST forcing, although consistent linkage between oceanic and atmospheric variables is evident. Further analytical and numerical studies on the generation of blocking are necessary, with considerations for the roles of atmospheric internal dynamics, surface boundary forcing due to snow cover and sea-ice and anomalous equatorial SST forcing associated with El Nino and La Nina events.

[35] **Acknowledgment.** This work is funded by the Korean Meteorological Administration Research and Development Program under Grant CATER 2012–3083 and CATER 2012–3100.

## References


Alexander, M. (2010), Extratropical air-sea interaction, sea surface temperature variability, and the Pacific Decadal Oscillation, in *Climate Dynamics: Why Does Climate Vary?*, *Geophys. Monogr. Ser.*, vol. 189, edited by D.-Z. Sun and F. Bryan, pp. 123–148, AGU, Washington, D. C., doi:10.1029/2008GM000794.

Barriopedro, D., R. Garcia-Herrera, A. R. Lupo, and E. Hernandez (2006), A climatology of Northern Hemisphere blocking, *J. Clim.*, *19*, 1042–1063, doi:10.1175/JCLI3678.1.

Buehler, T., C. C. Raible, and T. F. Stocker (2011), The relationship of winter season North Atlantic blocking frequencies to extreme cold or dry spells in the ERA-40, *Tellus, Ser. A*, *63*, 212–222.

Diao, Y., J. Li, and D. Luo (2006), A new blocking index and its application: Blocking action in the Northern Hemisphere, *J. Clim.*, *19*, 4819–4839, doi:10.1175/JCLI3886.1.

Ferreira, D., and C. Frankignoul (2005), The transient atmospheric response to midlatitude SST anomalies, *J. Clim.*, *18*, 1049–1067, doi:10.1175/JCLI-3313.1.

Frankignoul, C. (1985), Sea surface temperature anomalies, planetary waves and air-sea feedback in the middle latitudes, *Rev. Geophys.*, *23*, 357–390, doi:10.1029/RG023i004p00357.

Holopainen, E., and C. Fortelius (1987), High-frequency transient eddies and blocking, *J. Atmos. Sci.*, *44*, 1632–1645, doi:10.1175/1520-0469(1987)044<1632:HFTEAB>2.0.CO;2.

Huang, F., F. X. Zhou, and X. D. Qian (2002), Interannual and decadal variability of the North Pacific blocking and its relationship to SST, teleconnection and storm tracks, *Adv. Atmos. Sci.*, *19*, 807–820, doi:10.1007/s00376-002-0046-4.

Kalnay-Rivas, E., and L. O. Merkine (1981), A simple mechanism for blocking, *J. Atmos. Sci.*, *38*, 2077–2091, doi:10.1175/1520-0469(1981)038<2077:ASMFB>2.0.CO;2.

Kung, E. C., C. C. Dacamara, W. E. Baker, J. Susskind, and C. K. Park (1990), Simulations of winter blocking episodes using observed sea surface temperatures, *Q. J. R. Meteorol. Soc.*, *116*, 1053–1070, doi:10.1002/qj.49711649503.

Lau, N.-C., and M. J. Nath (1990), A general circulation model study of the atmospheric response to extratropical SST anomaly observed in 1950–79, *J. Clim.*, *3*, 965–989, doi:10.1175/1520-0442(1990)003<0965:AGCMSO>2.0.CO;2.

Lee, H.-S., and J.-G. Jhun (2006), Two types of the Asian continental blocking and their relation to the east Asian monsoon during the boreal winter, *Geophys. Res. Lett.*, *33*, L22707, doi:10.1029/2006GL027948.

Lejenäs, H., and H. Øakland (1983), Characteristics of Northerm Hemisphere blocking as determined from a time series of observaional data, *Tellus, Ser. A*, *35*, 350–362, doi:10.1111/j.1600-0870.1983.tb00210.x.

Liu, Q., N. Wen, and Z. Liu (2006), An observational study of the impact of the North Pacific SST on the atmosphere, *Geophys. Res. Lett.*, *33*, L18611, doi:10.1029/2006GL026082.

Liu, Z., and L. Wu (2004), Atmospheric response to the North Pacific SST: The role of ocean–atmosphere coupling, *J. Clim.*, *17*, 1859–1882, doi:10.1175/1520-0442(2004)017<1859:ARTNPS>2.0.CO;2.

Lupo, A. R. (1997), A diagnosis of two blocking events that occurred simultaneously over the midlatitude Northern Hemisphere, *Mon. Weather Rev.*, *125*, 1801–1823, doi:10.1175/1520-0493(1997)125<1801:ADOTBE>2.0.CO;2.

Matsueda, M., R. Mizuta, and S. Kusunoki (2009), Future change in Northern hemisphere wintertime atmospheric blocking simulated using a 20-km-mesh atmospheric global circulation model, *J. Geophys. Res.*, *114*, D12114, doi:10.1029/2009JD011919.

Nakamura, H., M. Nakamura, and J. L. Anderson (1997), The role of high and low-frequency dynamics in blocking formation, *Mon. Weather Rev.*, *125*, 2074–2093, doi:10.1175/1520-0493(1997)125<2074:TROHAL>2.0.CO;2.

Palmer, T. N., and S. Zhaobo (1985), A modelling and observational study of the relationship between sea surface temperature in the north-west Atlantic and the atmospheric general circulation, *Quart. J. R. Meteorol. Soc.*, *111*, 947–975, doi:10.1256/smsqj.47002.

Pelly, J. L., and B. J. Hoskins (2003), How well does the ECMWF ensemble prediction system predict blocking, *Q. J. R. Meteorol. Soc.*, *129*, 1683–1702, doi:10.1256/qj.01.173.

Peng, S., and J. S. Whitaker (1999), Mechanisms determining the atmospheric response to midlatitude SST anomalies, *J. Clim.*, *12*, 1393–1408, doi:10.1175/1520-0442(1999)012<1393:MDTART>2.0.CO;2.

Renwick, J. A., and J. M. Wallace (1996), Relationships between North Pacific wintertime blocking, El Nino, and the PNA pattern, *Mon. Weather Rev.*, *124*, 2071–2076, doi:10.1175/1520-0493(1996)124<2071:RBNPWB>2.0.CO;2.

Rex, D. F. (1950), Blocking action in the middle troposphere and its effect upon regional climate: The climatology of blocking action, *Tellus, Ser. A*, *2*, 275–301, doi:10.1111/j.2153-3490.1950.tb00339.x.

Rodwell, M. J., D. P. Rowell, and C. K. Folland (1999), Oceanic forcing of the wintertime North Atlantic Oscillation and European climate, *Nature*, *398*, 320–323, doi:10.1038/18648.

Shutts, G. J. (1983), The propagation of eddies in diffluent jetstreams: Eddy vorticity forcing of 'blocking' flow fields, *Quart. J. R. Meteorol. Soc.*, *109*, 737–761.

Thompson, D. W. J., and J. M. Wallace (1998), The Arctic Oscillation signature in the wintertime geopotential height and temperature fields, *Geophys. Res. Lett.*, *25*, 1297–1300, doi:10.1029/98GL00950.

Tibaldi, S., and F. Molteni (1990), On the operational predictability of blocking, *Tellus, Ser. A*, *42*, 343–365.

Tilly, D. E., A. R. Lupo, C. J. Melick, and P. S. Market (2008), Calculated height tendencies in a Southern Hemisphere blocking and cyclone event: The contribution of diabatic heating to block intensification, *Mon. Weather Rev.*, *136*, 3568–3578, doi:10.1175/2008MWR2374.1.

Trigo, R. M., I. F. Trigo, C. C. DaCamara, and T. J. Osborn (2004), Climate impact of the European winter blocking episodes from the NCEP/NCAR reanalyses, *Clim. Dyn.*, *23*, 17–28, doi:10.1007/s00382-004-0410-4.

Watanabe, M. (2001), Atmosphere–ocean feedback processes in the North Atlantic, paper presented at 11th Conference on Interaction of the Sea and Atmosphere, Am. Meteorol. Soc., San Diego, Calif.

Wiedenmann, J. M., A. R. Lupo, I. I. Mokhov, and E. A. Tikhonova (2002), The climatology of blocking anticyclones for the Northern and Southern Hemispheres: Block intensity as a diagnostic, *J. Clim.*, *15*, 3459–3473, doi:10.1175/1520-0442(2002)015<3459:TCOBAF>2.0.CO;2.